Identification of Yarn Periodical Errors Using Signal Processing Techniques Based on Capacitive and Optical Sensors Measurements

Vítor Carvalho[1,2], Filomena Soares[1]

[1]Dept. Industrial Electronics and Computers
[1]Minho University, [2]IPCA-EST
[1]Guimarães, [2]Barcelos, Portugal
(vcarvalho, fsoares)@dei.uminho.pt

Michael Belsley[3], Rosa Vasconcelos[4]

[3]Dept. Physics, [4]Dept. Textile Engineering
Minho University
[3]Braga, [4]Guimarães, Portugal
belsley@fisica.uminho.pt, rosa@det.uminho.pt

Abstract—This paper presents a study to identify the type and location of yarn periodical errors applying three different signal processing approaches based on FFT – Fast Fourier Transform, FWHT-Fast Walsh-Hadamard Transform and FDFI – Fast Impulse Frequency Determination. The errors determination is applied for the mass measurement of yarn using a capacitive sensor and for the measurement of yarn diameter/hairiness based on optical sensors. Commercial equipment uses exclusively a FFT approach which is not able to clearly detect other types of common periodical yarn errors, especially impulse errors, as well as an inferior resolution than the 1mm used in this work. The theoretical description of each signal processing technique is presented, as well as their application to several simulated errors, namely, sinusoidal, rectangular, pulse and impulse errors, showing proper results and a more complete analysis of periodical errors.

Keywords- capacitive sensors; optical sensors; periodical errors; yarn mass; yarn hairiness; yarn diameter; fast walsh-hadamard; fast impulse frequency determination; fft.

I. INTRODUCTION

The existence of yarn irregularities occurring with a constant frequency is a dominant source of imperfections in fabrics. These defects appear as high energy peaks in the frequency analysis [1-3] of yarn characteristics. So, with spectral analysis, it is possible to detect periodic errors in the yarn production process. Hairiness [4-7] (protruding fibers released from the main body of the yarn) (Figure 1) and irregularities (thin and thick places and neps) [1-3] (Figure 2a), are the major yarn parameters to be analyzed for the occurrence of periodical errors. However, there are two other types of errors [3, 8, 9]. The first type (Figure 2b) typically occurs due to the accumulated dirt at the stretching rollers in the drafting systems, or the displacement of the roller axis, producing a sinusoidal imperfection in the spun yarn diameter. The second type (Figure 2c) is generally due to imperfections in the surface of the rollers, generating a periodic impulse fault (imperfections in the raw material are seldom periodic).
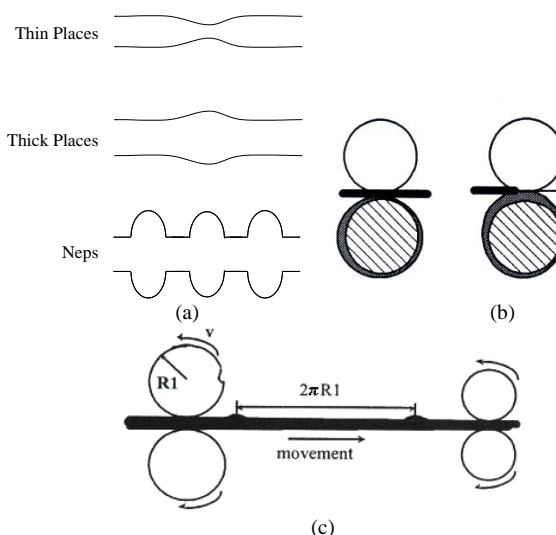

Figure 1. Yarn hairiness

Figure 2. (a) Yarn irregularities (b) Accumulated dirt error (c) Imperfection in the surface rollers error

To detect these yarn errors we have employed three different signal processing (SP) approaches [3] based on FFT (Fast Fourier Transform), FWHT (Fast Walsh-Hadamard Transform) and FDFI (Fast Impulse Frequency Determination), instead of a single strategy, based on FFT, as is the case for all current commercial solutions [1-3]. As most of the yarn periodical errors are sinusoidal they are easily detected by the FFT. It is our intention to explore the use of the FWHT, as an alternative to the FFT, as it has the advantage of requiring a lower computational effort when compared to the others The FDFI detects impulse errors, as they are not clearly identified by the other techniques. So, as

impulse errors could appear regularly, it was of major importance to present a viable solution for their detection.

This paper contains the following structure: the present Section I- identifies the problem and objectives of the paper; Section II - describes the sensors and the electronic/optical hardware employed for signals capture; Section III- describes the signal processing approaches used; Section IV- presents the results and Section V- presents the conclusions and future work developments.

II. THE MEASUREMENT SOLUTIONS DEVELOPED

To measure yarn irregularities, a parallel plates capacitive sensor was employed to detect yarn mass variations [3, 10, 11], while a coherent optical signal processing technique based on Fourier analysis together with an optical sensor was used to measure yarn hairiness [4-7]. The measurement of yarn irregularities can also be performed considering the yarn diameter variation [12-14]. All employed systems have a sample resolution of 1 mm (Figure 3).
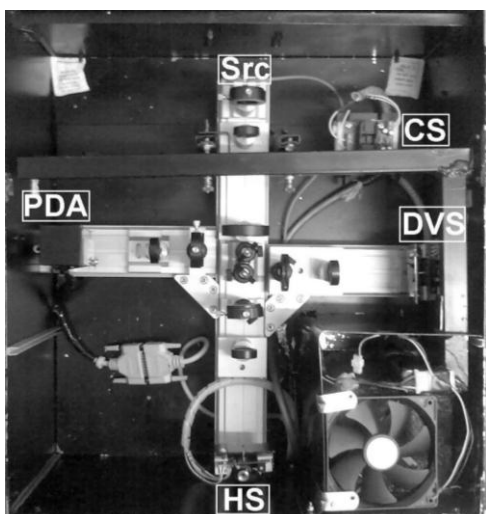

Figure 3.   Measurement systems (PDA - Photodiode Array (Diameter Characterization Sensor), DVS - Photodiode (Diameter Variation Sensor), HS - Photodiode (Hairiness Sensor), CS - Capacitor (Mass Variation Sensor), Src - Laser Source)

A.   Yarn Mass Variation System

The yarn mass variation system employed uses a 1 mm parallel plate capacitive sensor based on the integrated circuit MS3110 from Irvine Sensors, allowing direct yarn mass measurements over sample lengths of 1 mm. The sensor adopts a differential configuration to assure a higher robustness to variations in temperature, air humidity and pressure. It integrates transducer amplification and signal conditioning, as shown in Figure 4 [15]. This sensor has a resolution of capacity superior to 4 aF/rtHz, difficult to find in other commercial solutions, being compatible with the measurements of resolution in the order of aF needed for proper yarn mass quantification and variation.
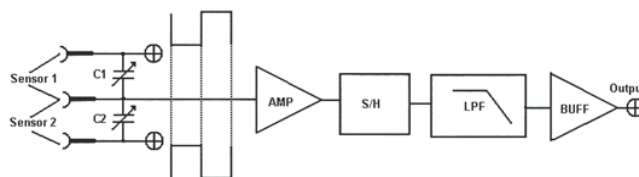

Figure 4.   Capacitive sensor configuration (C1,C2 – Adjustable capacitors to calibrate the sensors, AMP – Capacity to voltage converter and amplifier, S/H – Sample and hold, LPF – Two pole low pass filter, and BUFF – Output buffer)

B.   Yarn Diameter and Hairiness Quantification

The yarn diameter and hairiness quantification, based on two single photodiodes (S1227-1010BR from Hamamatsu) configured for a 1 mm sample length analysis, uses an optical setup with a low-pass spatial filter, to perform the diameter measurement (eliminating the influence of hairiness, Figure 5a), as well as with a high-pass spatial filter, to perform the hairiness measurement (eliminating the influence of the light which is not blocked by the yarn, Figure 5b) [15-18]. Figure 5c presents the optical hardware employed to determine yarn diameter and hairiness. A coherent optical imaging technique is employed to obtain an optical signal proportional to the amount of hairiness present on the yarn being sampled.

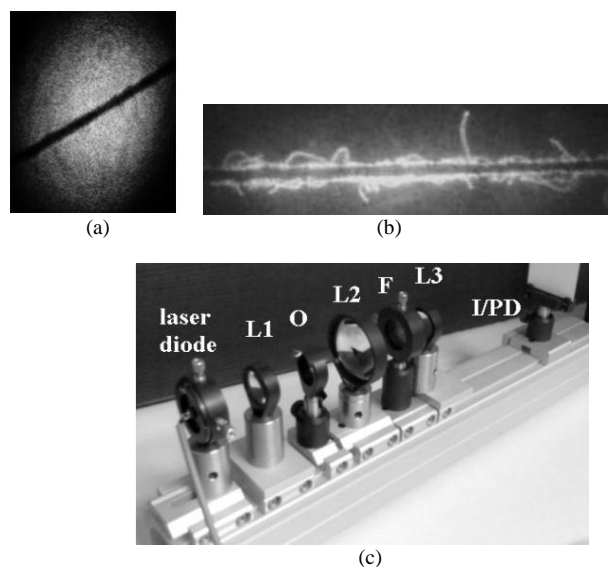(a)   (b)

(c)

Figure 5.   Example of an image resulting from the application of a (a) low-pass spatial filter, (b) high-pass spatial filter, (c) Custom developed optical yarn measurement hardware for a single direction

A diode laser (Eudyna FLD6A2TK) was used as an illumination source. This laser emits light at 685 ± 10 nm in both a single transverse and single longitudinal mode, with an especially low aspect ratio of 1.3. Emitting in a single longitudinal mode, the coherence length of the laser light is expected to be greater than several metres. The light from this laser was collimated using a single plano-convex lens of 40 mm focal length (L1). After illuminating the sample under study (O), the light passes through a 60 mm focal

length, 50 mm diameter plano-convex lens (L2) used to obtain the spatial Fourier transform of the object in its principal focal plane. A roughly 1 mm diameter opaque target (F) placed in the Fourier plane, blocks all spatial frequencies below 10 mm^{-1}, corresponding to a characteristic size of 100 microns or larger in the object plane. The filter is chosen to pass all of the relevant information regarding the small fibres, while almost entirely eliminating the nearly constant background light due to laser light that is not incident on the sample. However, the amount of light transmitted by the spatial filter is relatively small, roughly 3 to 4 orders of magnitude less than the full power emitted by the laser. A third plano-convex lens of 60 mm focal length (L3) is used to form a final filtered image (position of the photo detector in Figure 5c) (I/PD), which then highlights the sharp transitions in the object, basically the core boundary of the fibre and any small protruding hairs from the yarn core, allowing the measurement of hairiness. All lenses are 1 inch in diameter, except for the Fourier lens, L2, which is 2 inches in diameter. The lenses are carefully aligned to have a common optical axis. For the diameter measurements, basically the same optical hardware is used, with the exception that the high-pass spatial filter is replaced by a low-pass spatial filter, corresponding to a roughly 1mm diameter circular aperture, i.e., the complement of the high pass spatial filter. This filter blocks all spatial frequencies above 10 mm^{-1}, resultant to a characteristic size of 100 microns or less in the object plane. Afterwards, in order to obtain a voltage proportional to the brightness of the final image, a conditioning circuit was developed for yarn hairiness/diameter quantification. A high precision current to voltage converter based on a Burr-Brown operational amplifier OPA277P [19] was used between the output of the photodiode and the sampling board. Considering the hairiness and diameter measurement, the presented optical configuration overcomes the referred drawbacks of most available commercial methods [5, 20, 21]. The system also integrates a photodiode array (PDA in Figure 3), S8378-256Q from Hamamatsu, to allow a precise characterization of diameter and hairiness.

III. SIGNAL PROCESSING APPROACHES FOR DETECTION OF YARN PERIODICAL ERRORS

This section describes the signal processing techniques employed for detection of yarn periodical errors in diameter variation, mass variation and hairiness variation. In order to detect these errors, three different approaches are applied, namely, the FFT approach for sinusoidal errors, the FWHT approach for rectangular errors and the FDFI approach for impulse errors. The results obtained are shown in terms of wavelengths ($\lambda(m)$), calculated according to (1) [2], as they give a more perceptive result to the yarn producer.

$$\lambda = L_{sample} \frac{f_a}{1000 f_d} \tag{1}$$

where, L_{sample} is the sample length (mm), f_a is the acquisition frequency (Hz) and f_d is the detected faults frequencies (Hz).

A. FFT Approach

The first approach is based on the FFT transform [11-13] with a narrow bands definition to aggregate the harmonics, due to the highly concentrated information of the spectrum. This can be considered a periodgram. All the wavelengths detected at the corresponding energy band, are added and then multiplied by the number of detected wavelengths, obtaining the final value of the energy band (2) [1, 10].

$$e(j) = k_e \sum_{w=1}^{w=k_e} \lambda(w) \tag{2}$$

where, k_e is the number of detected wavelengths in the band, w is the index of the detected wavelength and λ is the wavelength amplitude at the index w.

B. FWHT Approach

The Walsh functions create an ordered set of rectangular waves presenting only two possible amplitudes, +1 and -1 [14, 15]. Walsh functions are commonly classified using a notation in terms of odd and even symmetries. Two series are presented, the CAL series (even) and the SAL series (odd), which are very similar to the trigonometric series COSIN and SIN, respectively. The Hadamard order is the one used in this work, as it is computationally the most efficient. The Walsh Hadamard transform is given by (3).

$$FWHT = \begin{bmatrix} X(0) & X(1) & ... & X(n_s-1) \end{bmatrix}^{n_w} WH \tag{3}$$

where, X is the array of signal variation $(0,...., n_s-1)$, n_s is the number of samples, n_w is the order of the WH matrix.

C. FDFI Approach

The FFT and FWHT do not achieve good results in detecting impulse errors: the FFT cannot detect them and the FWHT do not distinguishes them from other errors. So, a new approach, Fast Impulse Frequency Determination (FDFI) [1, 8-10] was considered. In the impulse error presented in Fig. 2, if there are stretching rollers in addition to those responsible for the error, the error will be extended, causing an impulse error with a longer width. The FDFI Transform was developed [1, 8-10] to detect this kind of fault, following an approach which consists of the multiplication of an error signal by a coefficient matrix. The error signal is obtained comparing each sample with a predefined threshold. If the sample amplitude is outside the threshold, the error signal takes the '1' value, otherwise, it takes the value '0'. Afterwards, a matrix is generated, where all the admissible error periods and phases (initial points) are tested (from n_s / 2 to $(n_s$ / 4$) + 1$). As the n_s / 4 period is multiple of the n_s / 2 period, it is not necessary to test it.

IV. RESULTS OF SIGNAL PROCESSING TECHNIQUES WITH SIMULATED ERRORS

A study on the application of signal processing techniques to simulated periodical errors in a hairiness variation signal [10] is presented. Periodical errors tested: sinusoidal error with amplitude of 20 % (Figure 6a); positive periodic rectangular error with amplitude of 40 % (Figure 6b); a pulse error with amplitude of 100 % (Figure 7a) and a periodic impulse error with amplitude of 400 % every 384 samples (Figure 7b).
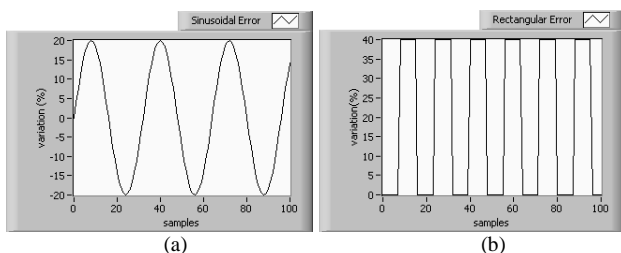
Figure 6.   (a) Zoomed sinusoidal error and (b) positive rectangular error added to the original signal (Figure 8)
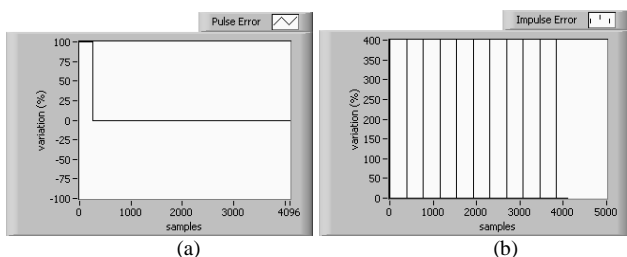
Figure 7.   (a) Pulse errors and (b) periodic impulse error added to the original signal (Figure 8)

A. Original Signal

In order to test the signal processing approaches it was considered a real acquired signal: Figure 8 - original signal, is based on the signal of hairiness of a 100% cotton yarn measured by the photodiode DS (Figure 3). It considers the variation (%) of each sample of 1mm in reference to the average of hairiness measured. The results of FFT and FWHT of Figures 9-16 present normalized results in the Y-axis.
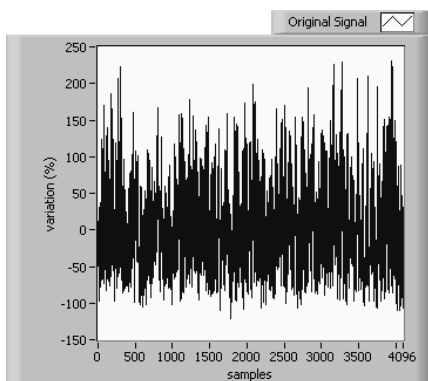
Figure 8.   Original signal

B. Original Signal with a Sinusoidal Error Added Analysis

Figures 9 and 10 present the results of FFT and FWHT approach for this situation, respectively.
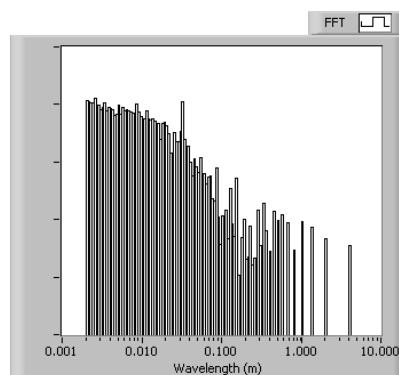
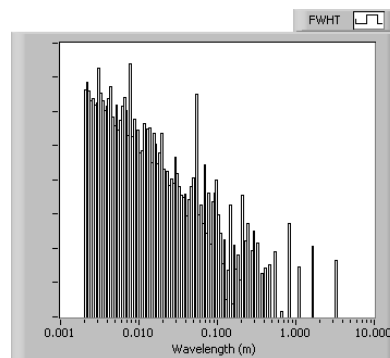Figure 9.   FFT result for the original signal with the sinusoidal error

Figure 10.   FWHT result for the original signal with the sinusoidal error

Analysing Figure 9 (FFT), it is verified that a relevant protruding peak is now observed around 3 cm, detecting as expected, a clear sinusoidal error at this wavelength. The FWHT spectrogram Figure 10 also presents, mainly, two new protruding peaks around 3 mm and 6 cm. So, as expected, it can be verified that a sinusoidal error is also detected by the FWHT, but in several narrow bands. As known when an error does not match a tested waveform of the applied signal processing technique, it is reflected over several waveforms at different (usually harmonic) wavelengths (decomposition).

C. Original Signal with a Rectangular Error Added Analysis

Figures 11 and 12 present the results of FFT and FWHT approach for this situation, respectively.
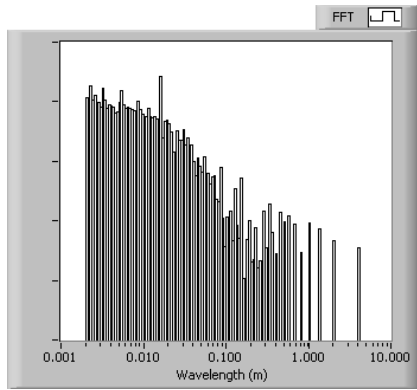
Figure 11. FFT result for the original signal with the rectangular error
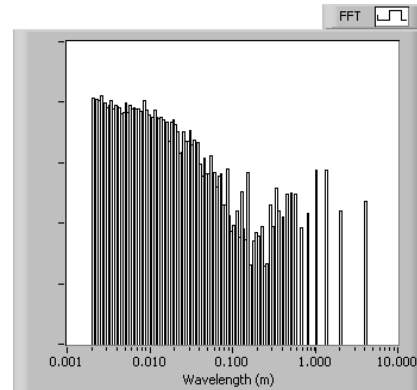

Figure 13. FFT result for the original signal with the pulse error
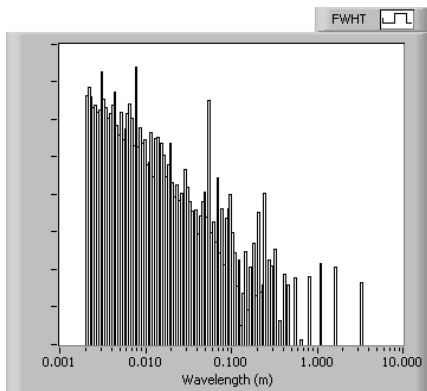

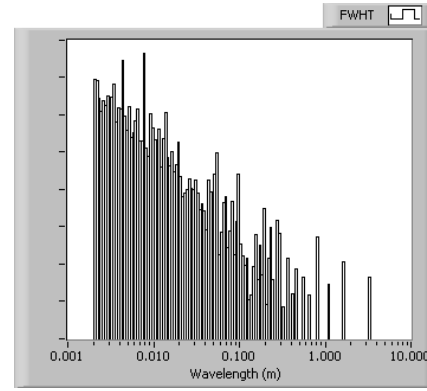Figure 12. FWHT result for the original signal with the rectangular error

Figure 14. FWHT result for the original signal with the pulse error

Figure 11 (FFT) contains a relevant protruding peak at around 2 cm and three others peaks, with minor amplitudes at wavelengths near 2 mm, 3 mm and 5 mm. As expected, it can be verified that a rectangular error is also detected by the FFT over several narrow bands in which the main error component clearly protrudes over the spectrogram. The FWHT spectrogram (Figure 12) also presents several new protruding peaks around 3 mm and 5 mm, 3, 5, 7, 10, 25 cm. However, the more relevant new protruding peaks are at wavelengths 3 mm, 5 cm and 25 cm. So, it can be verified that a periodic rectangular error is also detected over several bands by the FWHT as in the FFT, probably because the added rectangular error does not completely match a tested FWHT waveform. However, in the FWHT the protruded peaks which are also detected in the FFT have higher amplitudes, due to its close similarity to the FWHT waveforms.

D. Original Signal with a Single Pulse Error Added Analysis

Figures 13 and 14, present the results of FFT and FWHT approach for this situation, respectively.

No new protruding peaks are observed in Figure 13 (FFT), highlighting that this technique is not at all sensitive to pulse errors. This situation was expected because it is a non-periodic error. In FWHT (Figure 14) a new protruding peak is observed around 5 mm probably because the simulated error matched a tested waveform of the FWHT technique. It can be concluded that the FWHT could be useful to detect pulse errors.

E. Original Signal with a Periodical Impulse Error Added Analysis

Figures 15 and 16 present the results of FFT and FWHT approach for this situation, respectively. As no new protruding peaks are observed in Figure 15 (FFT), this technique seems to be unhelpful to detect impulse errors. In FWHT (Figure 16), several alterations are observed: the main protruding peak of the spectrogram around 8 mm as well as several other, were severely reduced while a new protruding peak is observed around 2.5 mm. Finally, a reinforcement of the amplitude of the protruding peak around 8 cm occurred. It can be concluded that although the FWHT detects this type of error, it is impossible to distinguish it, in the spectrogram, from the pulse error. So the use of the FDFI is now considered.
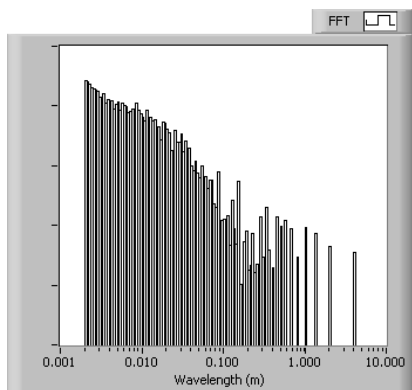
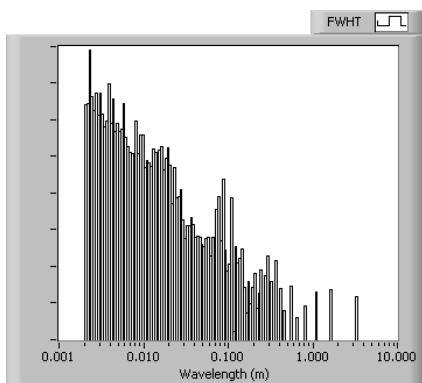Figure 15. FFT result for the original signal with the impulse error

Figure 16. FWHT result for the original signal with the impulse error

Table I presents the signal processing results based on FDFI, tested for impulse errors with a threshold of 300 % showing their initial position, period and number of impulses

TABLE I. DESCRIPTION OF THE DETECTED IMPULSE ERRORS

100 % error row	Initial position (sample)	Period (samples)	Number of impulses
254016	0	1920	3
254400	384	1920	2
254784	768	1920	2
255168	1152	1920	2
255552	1536	1920	2
917760	0	1536	3
918144	384	1536	3
918528	768	1536	3
918912	1152	1536	2
1434048	0	1152	4
1434432	384	1152	4
1434816	768	1152	3

As it can be seen in Table I, it is verified that the signal error is decomposed in 12 error rows, with initial positions in indexes 0, 384, 768, 1152 and 1536, containing periods of 1152, 1536 and 1920 samples, resulting in a number of impulses between 2 and 4.

V. CONCLUSION AND FUTURE WORK

Different signal processing techniques based on FFT, FWHT and FDFI were tested using an experimental hairiness spectrogram for error detection. Artificial sinusoidal, rectangular, pulse or periodical impulse errors were added to the original signal. The previously described analysis allows us to conclude that: periodic sinusoidal errors are clearly distinguished using the FFT approach over a narrow band and in the FWHT over several bands where the main components are visible in the spectrum; periodic rectangular error is distinguished in the FFT approach over several bands, where the main error component clearly extends above the spectrum and in the FWHT, also over several bands, if the error does not match the tested waveforms of the technique (if a match is verified a clearly narrow band will protrude); pulse or periodic impulse errors are not detected by the FFT approach but are detected by the FWHT over a narrow band, considering the pulse error and over several bands considering the periodic impulse error. However, it is difficult to distinguish, an impulse error from a pulse error. For this it is more suitable to use an FDFI analysis; periodic impulse errors are clearly detected by the FDFI approach.

The performance allowed by the FWHT in comparison to the FFT, is supported by the computational effort reduction associated to the less complex calculation of rectangular square waves in comparison to sinusoidal waves.

For a complete analysis of given yarn with unknown error, we recommend the use of all three signal processing techniques as they are in many sense complementary.

Future work will include the development of new optimized FDFI algorithms in order to reduce the associated computational effort as well as studies that allow the use of the FWHT in replacement of the FFT.

REFERENCES

[1] V. Carvalho, "Parametrização de Fio Têxtil Baseada na Análise de Massa", Msc Thesis, Minho University, Guimarães, 2004 (in Portuguese).

[2] R. Furter, "Evenness Testing in Yarn Production: part I", The Textile Institute and Zellweger Uster AG, Manchester, 1982.

[3] J. Neves, "A Irregularidade dos Fios Têxteis, Sua Origem, Medição e Análise", Oporto, 1968.

[4] B. Goswami, J. Martindale, and F. Scardino, "Textile Yarns: Technology, Structure and Applications", 2nd Edition, John Wiley & Sons, New York, 1977.

[5] V. Carvalho, P. Cardoso, M. Belsley, R. Vasconcelos, and F. Soares, "Yarn Hairiness Parameterization Using a Coherent Signal Processing Technique", Sensors and Actuators A: Physical, Vol. 145 (1), 2008, pp. 217-224.

[6] V. Carvalho, P. Cardoso, M. Belsley, R. Vasconcelos, and F. Soares, "Optical Yarn Hairiness Measurement System", INDIN 2007, 5th IEEE Conference on Industrial Informatics, 23-27 July, Vienna, Austria, 2007.

[7] V. Carvalho, P. Cardoso, M. Belsley, R. Vasconcelos, and F. Soares, "Yarn Irregularity Parameterization Using Optical Sensors", Fibres and Textiles in Eastern Europe, Vol. 17, N.º 1 (72), 2009, pp. 26-32.

[8] J. Monteiro, "Sistema Distribuído de Análise da Regularidade de Fios Têxteis", PhD Thesis, Minho University, Braga, 1990 (in Portuguese).

[9] J. Monteiro and C. Couto, "Pulse Frequency Calculation and Estimation in Yarn Evenness Analysis", IEEE Industrial Electronics Society, Orland, USA, 1995.

[10] V. Carvalho, P. Cardoso, M. Belsley, R. Vasconcelos, and F. Soares, "Optical Yarn Hairiness Measurement System", INDIN 2007, 5th IEEE Conference on Industrial Informatics, 23-27 July, Vienna, Austria, 2007.

[11] V. Carvalho, "Automatic Yarn Characterization System", PhD Thesis, Minho University, Braga, 2008.

[12] V. Carvalho, M. Belsley, R. Vasconcelos, and F. Soares, "Automatic Yarn Characterization System: Design of a Prototype", IEEE Sensors Journal, Vol. 9 (8), 2009, pp. 987-993.

[13] V. Carvalho, J. Monteiro, R. Vasconcelos, and F. Soares, "Yarn Mass Analysis With 1 mm Capacitive Sensors", ISIE2004, 4-7 May, Ajjacio, France, 2004.

[14] V. Carvalho, M. Belsley, R. Vasconcelos, and F. Soares, "Yarn Periodical Errors Determination Using Three Signal Processing Approaches", (submitted for publication in Journal of Signal Processing Systems).

[15] V. Carvalho, M. Belsley, R. Vasconcelos, and F. Soares, "Automatic Yarn Characterization System", IEEE Sensors 2008, 7th IEEE Conference on Sensors, 26-29 October, Lecce, Italy, 2008.

[16] V. Carvalho, P. Cardoso, M. Belsley, R. Vasconcelos, and F. Soares, "Yarn Diameter Measurements Using Coherent Optical Signal Processing", IEEE Sensors Journal, Vol. 8 (11), 2008, pp. 1785-1793.

[17] A. Barella, "Yarn Hairiness", Textile Progress Journal, Vol. 13 (1), 1981, pp. 1-57.

[18] V. Carvalho, P. Cardoso, M. Belsley, R. Vasconcelos, and F. Soares, "Yarn Hairiness Characterization Using Two Orthogonal Directions", IEEE Trans. Instrumentation & Measurement, Vol. 58 (3), 2009, pp. 594-601.

[19] url:http://pdf1.alldatasheet.com/datasheet-pdf/view/56757/BURR-BROWN/OPA277.html (access in June 2012)

[20] V. Carvalho, P. Cardoso, M. Belsley, R. Vasconcelos, and F. Soares, "Yarn Diameter Measurements Using Coherent Optical Signal Processing", IEEE Sensors Journal, Vol. 8(11), 2008, pp. 1785-1793.

[21] V. Carvalho, P. Cardoso, M. Belsley, R. Vasconcelos, and F. Soares, "Yarn Diameter Characterization Using Two Orthogonal Directions", Journal Experimental Techniques, Vol. 35 (5), 2011, pp. 7-15.